Modeling and Experimental Analyses of a Two-Cell Polymer Electrolyte Membrane Fuel Cell Stack Emphasizing Individual Cell Characteristics

Sang-Kyun Park[1]
e-mail: parksan@auburn.edu

Song-Yul Choe
e-mail: choe@eng.auburn.edu

Mechanical Engineering Department,
Auburn University,
Auburn, AL 36848

Performance of individual cells in an operating polymer electrolyte membrane (PEM) fuel cell stack is different from each other because of inherent manufacturing tolerances of the cell components and unequal operating conditions for the individual cells. In this paper, first, effects of different operating conditions on performance of the individual cells in a two-cell PEM fuel cell stack have been experimentally investigated. The results of the experiments showed the presence of a voltage difference between the two cells that cannot be manipulated by operating conditions. The temperature of the supplying air among others predominantly influences the individual cell voltages. In addition, those effects are explored by using a dynamic model of a stack that has been developed. The model uses electrochemical voltage equations, dynamic water balance in the membrane, energy balance, and diffusion in the gas diffusion layer, reflecting a two-phase phenomenon of water. Major design parameters and an operating condition by conveying simulations have been changed to analyze sensitivity of the parameters on the performance, which is then compared with experimental results. It turns out that proton conductivity of the membrane in cells among others is the most influential parameter on the performance, which is fairly in line with the reading from the experimental results.
[DOI: 10.1115/1.2972165]

Keywords: PEMFC, stack, individual cell, cell voltages, modeling

1 Introduction

Polymer electrolyte membrane fuel cell (PEMFC) is the highest potential candidate among other fuel cell technologies because of low operating temperature, a relatively short start-up time, and a high power density. Applications of this technology include vehicles, utilities, and portable electronics.

A fuel cell stack is constructed by attaching cells in series that are composed of functional component layers. The layers serve to provide pathways for reactants, charges, and water and heat as by-products. The complexity of transport mechanism of the mass and charges and chemical reactions in the device subject to a varying temperature environment presents a challenging issue that has not been fully understood, even though the experimental and theoretical analyses have been published. Particularly, most of the experimental research conducted in the past years has been based on analyses of the performance of either a single cell or the whole stack simply by measuring the voltage under operation conditions.

In reality, the performance of the individual cells in a stack varies depending on designs, locations, and operating conditions, to name a few. Thus, the cell voltages of a single cell or a stack are experimentally investigated to find out causality subject to various operating conditions. The key parameters considered include the working temperature of the stack, humidity on the air stream, pressure, and stoichiometric ratio.

The different studies conducted [1] have shown that distribution of the temperature in a stack is not uniform. It is dynamically changed under the influence of different heat source terms in the layers. At the same time, the variation of the temperature influences the exchange current density, gas diffusivity, membrane conductivity, and water condensation as well as evaporation. The higher the working temperature in the stack is, the more reactive the chemical reaction becomes. Consequently, the cell performance is improved. In contrast, the high temperature decreases proton conductivity in the membrane by dehydration and subsequently a high Ohmic overpotential. [2–11].

The air stream should be properly humidified to balance between water produced, taken up by protons in the membranes and exited at the outlet. Specifically, the balance of water content in the membrane is of importance for protons to keep high conductivity that enables the efficiency to be high and the heat produced to reduce [2–6,12–14]. On the other hand, the temperature of the supplied gas affects the vapor mass residing in the air. At an elevated temperature of the supplied gas, this might cause dehydration of the membrane or water flooding dependent on the current density and working temperature of the cells [3–6,12,15].

The operating pressure directly influences the partial pressure of the reactant. At a high operating pressure, the partial pressure drop in the gas diffusion layer (GDL) gets less and the reaction rate in the catalyst gets higher and as a result the performance of a cell gets improved. In addition, a high pressure can steadily supply the reactant required for a high current load, which secures a safe operation [2–7,16].

In addition, the air stoichiometric ratio influences not only the oxygen available for the reactions but also the removal of water produced, which subsequently affects the water content in the membrane. Specifically, an increase of the flow rate at a high current load can potentially repel more water than the produced.

[1]Corresponding author.

Manuscript received June 17, 2007; final manuscript received October 4, 2007; published online November 18, 2008. Review conducted by Ugur Pasaogullari.

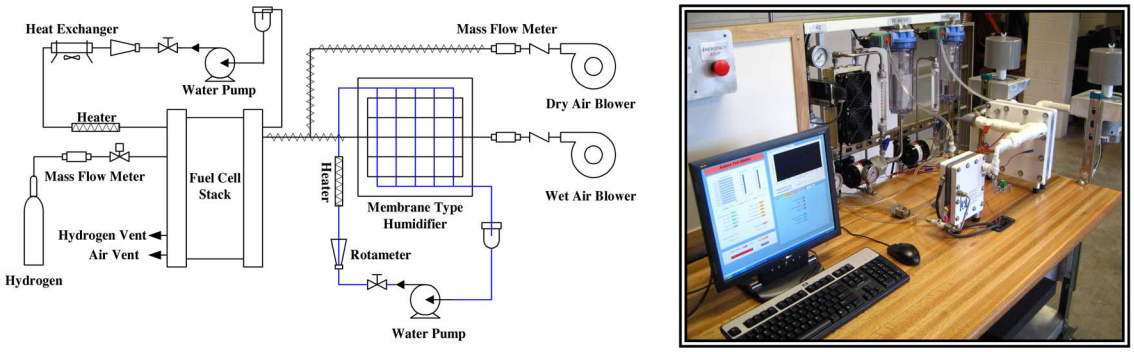

Fig. 1 Schematic of experimental apparatus

As a result, water in the membrane can be imbalanced and the membrane is likely to be dehydrated, even though the availability of oxygen increases the reaction rate in the catalyst. [2,4,12,15,7].

The effects of the operating conditions on the performance of the individual cell of the stack have been studied by comparison of changes in Ohmic voltage drop, impedance of a stack, individual cell voltages, or a combination of them. However, the measured quantities do not provide a clear causality between the operating conditions and the consequent performance. Thus, it is hard to obtain standardized codes for assessment of the performance of a stack. Characterization and evaluation of the cells in a stack subject to different operating conditions are generally performed by measurement of polarization curve or impedance. Measurement of an Ohmic voltage drop in the individual cells used by Tuomas et al. [17] is a method that a current interruption is applied to estimate the conductivity of the cells and assess the performance of the cells under conditions of a free and forced convection of air supply and current density. However, the study does not consider any other operating conditions. Xiaozi et al. [18] employed the electrochemical impedance spectroscopy (EIS) to measure the impedance and Ohmic resistance of the individual cells. However, the only one operating condition varied is the load current density by using an E-load. Paul et al. [19] employed the polarization curve to assess the effects of designs and operating factors on distribution of the cell voltage across the stack. The results showed that the *I-V* characteristics of the individual cells are influenced by temperature distribution, degradation, and tolerance of the components as well as the design parameter of the flow patterns. The only operating condition considered for the experiment is the load current.

Studies conducted in this paper focus on the experimental and computational analyses of a two-cell stack. The individual cell voltages are measured under the variation of three different operating conditions: (1) working temperature of the stack, (2) temperature of the supplying air at the inlet, and (3) stoichiometric ratio. In fact, the relationship between the distributions of the cell voltages in a stack and other influencing factors has not been clearly defined. In addition, most of the physical quantities necessary for measurements are not accessible under operating environments. Thus, modeling techniques are employed to study influences of design parameters and operating conditions on performance. The model developed is based on voltage equations for the cells, energy equation with heat source terms in each layer, mass conservation in the membrane, and diffusion in the GDL considering a two-phase phenomenon for water. The stack for the study is a two-cell stack with a separator in the middle of the stack to minimize influence of temperature of the neighboring cells. Simulated results are compared with the experiments.

2 Experimental Apparatus and Method

2.1 Apparatus. The schematic of the experimental setup is depicted in Fig. 1. The test equipment is devised to test a PEM fuel cell system that consists of a two-cell stack and the balance-of-the-plant that includes an air supply, a humidifier, a hydrogen delivery system, a coolant circuit, controls, and an E-load. Instrumentations are implemented by the LABVIEW installed on a personal computer (PC).

The air at the inlet of the stack is supplied by two air blowers. The air and humidification system mixes a dry air stream and a humidified air stream together to achieve a targeted relative humidity and temperature prior to entering the fuel cell. The hydrogen was automatically supplied through the mass flow meter proportional to the load current generated. The coolant is controlled by an electrical pump to keep the temperature of the coolant channel outlet of the stack. Thus, the working temperature can be assumed to be the same as to the temperature of the coolant water in the outlet.

The stack is constructed with two cells separated by a thermally conductive plate in order to minimize the potential influences of the coolants on the working temperature. Other components used in the cells are the same as those in a typical assembly. The cell fabricated has an active area of 140 cm^2. The membrane and the GDL have thicknesses of 0.035 mm and 0.4 mm. The plate for the gas flow channel is 1.5 mm thick and made of TM graphite. The plates for the coolant channels and the separator are made of graphite, thicknesses of which 3 mm and 1.5 mm. The thicknesses of the endplate and the bus plate are 28.5 mm and 1.5 mm, respectively. The maximum electric power of the stack is 80 W.

2.2 Experimental Conditions and Measurement. For measurement of the voltage in the individual cells, a wire lead is connected to the separator so that the voltages between the separator and the bus plates can be measured. When controlling the current drawn from the E-load, the voltage at the lead gives a *I-V* characteristic of the individual cells. Operating conditions that changed for the experiment are as follows: (1) working stack temperature (T_{st}), (2) air temperature (T_{air}), and (3) air stoichiometric ratio (air_{stoich}), which is summarized in Table 1. The hydrogen is supplied as a dry gas under a room temperature. The stoichio-

Table 1 Experimental conditions

Supply air temperature (°C)	30 (a1), 40 (a2), 50 (a3), 60 (a4)
Stack operating temperature (°C)	40 (b1), 50 (b2), 60 (b3)
Air stoichiometric ratio	2 (c1), 3 (c2), 4 (c3)
Relative humidity of air (%)	100

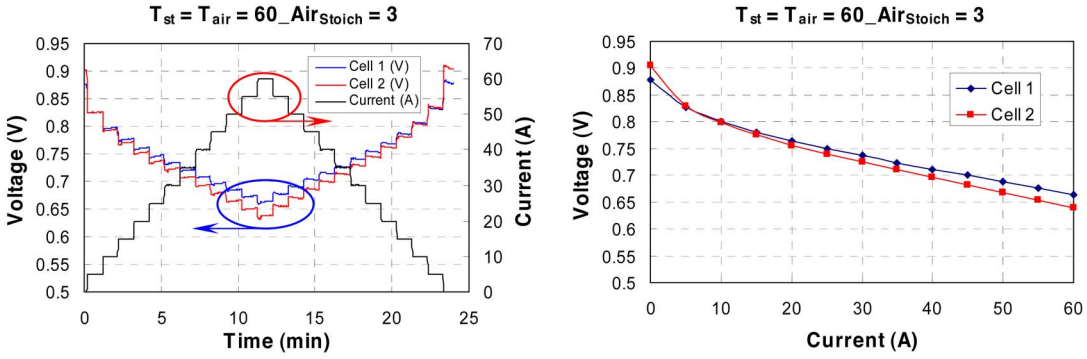

Fig. 2 Output voltages and *I-V* curves of the two cells at a multiple step current

metric ratio for the hydrogen is set to be 1.2 over the whole range of the load current. The air is fully humidified and the stoichiometric ratio is set according to the load current.

Experiments have been carried out with the following steps. First, the coolants are heated up and then circulated through the stack until the outlet temperature of the stack takes a stable and constant temperature. Then, it is assumed as initial working temperature of the stack. The experiments are started by applying a load current, after the temperature, the flow rate, and the relative humidity of the air set by the blowers get stabilized. In addition, the anodic side is purged for a period of 1 s in every 3 min to remove water backdiffused from the cathode side and minimize a subsequent voltage drop.

Figure 2 shows the voltage and current wave form at the two cells with respect to time (a) and an *I-V* characteristic (b) at a profile of a load current. The operating conditions are $T_{st}=T_{air}=60°C$, $air_{stoich}=3$, and RH=100%. The load is a multiple step current, whose magnitude varies from 0 A to 60 A with duration of one minute. The output voltage is a mean value of the two voltages measured at the positive and negative edges of each current step. The results show a clear trend that there exists a voltage difference between the two cells that might be caused from various reasons aforementioned.

3 Model Setup

The model is based on empirical *I-V* equations that describe static behaviors of a cell and takes into account four additional major effects: The water balance in the membrane, the gas dynamics in the gas diffusion layer, the temperature distribution in a cell, and a new GDL model with a two-phase phenomenon for water described below. A cell is constructed by a connection of individual model for layers, as shown Fig. 3. A separator is used for the coolant channel between two cells to minimize the cooling effects on performance of the two adjunct cells.

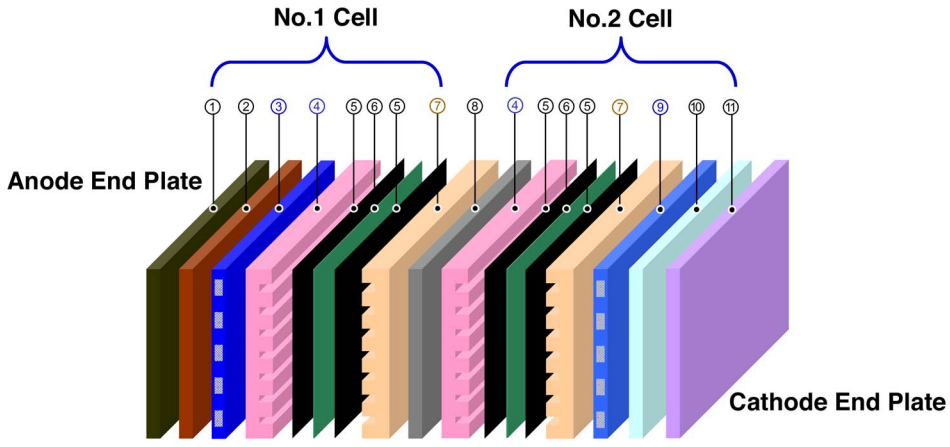

①	Anode End Plate	⑦	Cathode Gas Channel Plate
②	Anode Bus Plate (Current collector)	⑧	Separator (No coolant channel)
③	Anode Cooling Plate	⑨	Cathode Cooling Plate
④	Anode Gas Channel Plate	⑩	Cathode Bus Plate (Current collector)
⑤	Gas Diffusion Layer	⑪	Cathode End Plate
⑥	Anode Catalyst, MEA, Cathode Catalyst		

Fig. 3 Schematic simulation domain for a two cell stack model

3.1 Model Equations

3.1.1 Stack Voltage. The *I-V* characteristic is given by the difference between the open circuit voltage E and the overpotentials that include the activation overpotential in the catalyst on the cathode side η_{act}, the Ohmic overpotential in the membrane η_{ohm}, and the concentration overpotential η_{con}. The stack voltage for the two cells is obtained by simply adding the voltages of Cells 1 and 2:

$$V_{cell} = E - \eta_{act} - \eta_{Ohmic} - \eta_{conc}$$

$$V_{stack} = V_{Cell\ 1} + V_{Cell\ 2} \tag{1}$$

The open circuit potential E is calculated from the energy balance between the chemical energy and the electrical energy [11].

$$E = 1.229 - 0.85 \times 10^{-3}(T - 298.15) + 4.3085 \times 10^{-5} T\left[\ln(p_{H_2}) + \frac{1}{2}\ln(p_{O_2})\right] \tag{2}$$

The activation overpotential η_{act} can be expressed as a function of the working temperature and the oxygen concentration [11].

$$\eta_{act} = \xi_1 + \xi_2 T + \xi_3 T \ln(c_{O_2}) + \xi_4 T \ln(I) \tag{3}$$

where ξ_i is the constant parametric coefficients, I is the current (A), and c_{O_2} is the oxygen concentration. The Ohmic overvoltage η_{Ohm} [14,20] is calculated from Ohm's law:

$$\eta_{ohm} = I \cdot R_{ohm} = \frac{I \cdot t_{mem}}{\sigma_{mem}} \tag{4}$$

where R_{Ohm} is the Ohmic resistance, and t_{mem} and σ_{mem} are the membrane thickness and conductivity, respectively.

The variation of the membrane conductivity is given in the form [14,20]

$$\sigma_{mem} = \sigma \cdot \exp\left[1268\left(\frac{1}{303} - \frac{1}{T}\right)\right]$$

$$\sigma = 0.005139\lambda_{mem} - 0.00326 \tag{5}$$

where λ_{mem} is the membrane water content.

The concentration overvoltage, η_{con} [21] is given by the following equation:

$$\eta_{con} = -b\ln\left(1 - \frac{I}{I_{max}}\right) \tag{6}$$

where b is a parametric coefficient (V) that depends on an operation state in the cell, I is the actual current density (A/cm^2), and I_{max} is the maximum current density (A/cm^2).

3.1.2 Gas Diffusion Layer with a Two-Phase Phenomenon for Water. The phase of water in the GDL plays a significant role in transport of water and reactants. The model for the GDL considers the mass transport in gas and liquid phases and the phase transition between liquid water and water vapor. Figure 4 shows a new setup how the GDL model is modified to consider the two phase. The GDL on the cathode side is fictitiously divided into three control volumes because of a required minimum number of domains necessary for calculating a distribution in the layer.

Most of dynamic model proposed for the GDL assumed that water generated and supplied are vapor, so that effects of the liquid water are generally neglected. When the liquid water is involved, diffusion characteristics are different from those with the vapor state. The diffusion in the GDL can be redefined by introducing an effective diffusivity that describes diffusion behavior of vapor and liquid water in a capillary [22,23]. No tortuosity has been considered:

$$\langle D_j \rangle = D_j \varepsilon \left(\frac{\varepsilon - 0.11}{1 - 0.11}\right)^{0.785}(1 - s)^2$$

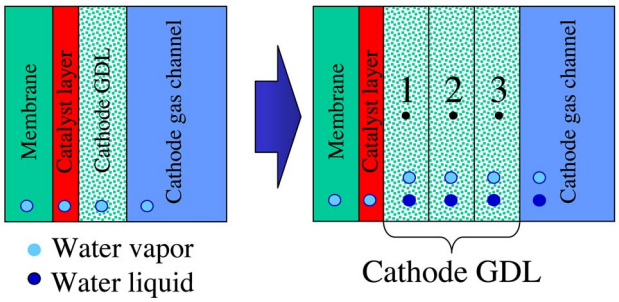

Fig. 4 Schematic domain for the GDL with a two-phase phenomenon

$$\varepsilon = \frac{V_p}{V}, \quad s = \frac{V_l}{V_p}$$

$$j = O_2, \text{vapor} \tag{7}$$

where $\langle D_j \rangle$ is the effective diffusivity (m^2/s), D_j is the diffusion coefficient (m^2/s) at a single phase, ε is the porosity of the diffusion layer, s is the liquid water saturation ratio, V_p is the pore volume of the GDL (m^3), V is the total volume of the GDL (m^3), and V_l is the volume of the liquid water (m^3).

3.1.3 Membrane. The water content in the membrane determines the proton conductivity. The dynamics of the water content is described by two effects; the electro-osmotic driving force by the different electrochemical potential at the anode and cathode and the diffusion caused by the water concentration gradient at the two boundaries. Considering the water mass flows at the boundaries of the membrane layer, the dynamic of the water concentration in the membrane can be improved as follows [24]:

$$\lambda_{mem} = \frac{C_{H_2O,mass}/M_{H_2O}}{\frac{\rho_{dry,mem}}{M_{mem}} - b \cdot C_{H_2O,mass}/M_{H_2O}}$$

$$\dot{m}_{water,mem} = \frac{d(C_{H_2O,mass} A_{cell} t_{mem})}{dt} = W_{ele,mem,anode} - W_{ele,mem,cathode} + W_{diff,mem,anode} + W_{diff,mem,cathode} \tag{8}$$

where C is the mass concentration (kg/m^3), M is the mole mass (kg/mol), ρ is the membrane dry density, and A_{cell} is the fuel cell area (m^2).

3.1.4 Energy Balance. If a cell is assembled with cubical layers, thermophysical properties of which are isotropic and constant, then according to the energy conservation equation, the total energy changes in a controlled volume are equal to the sum of energy exchange at boundaries and internal energy resources. In fact, the energy exchanges at boundaries occur by two factors: (a) the conduction across the cell and (b) the convection occurring between bipolar plates with the coolant, the reactants, and water. Thus, the thermal-dynamic behavior can be described with the following energy conservation equation [24]:

$$\sum_i Cp_i C_{i,mass} A_{cell} t_{cv} \frac{dT_{cv}}{dt} = \underbrace{\sum W_{in} A_{cell} Cp_j (T_{in} - T_{cv})}_{\text{mass flow in}} + \underbrace{\dot{Q}_{conv} A_{cell}}_{\text{convection heat transfer}} + \underbrace{\dot{Q}_{cond} A_{cell}}_{\text{conduction heat transfer}} + \underbrace{\dot{Q}_{sou}}_{\text{sources}} \tag{9}$$

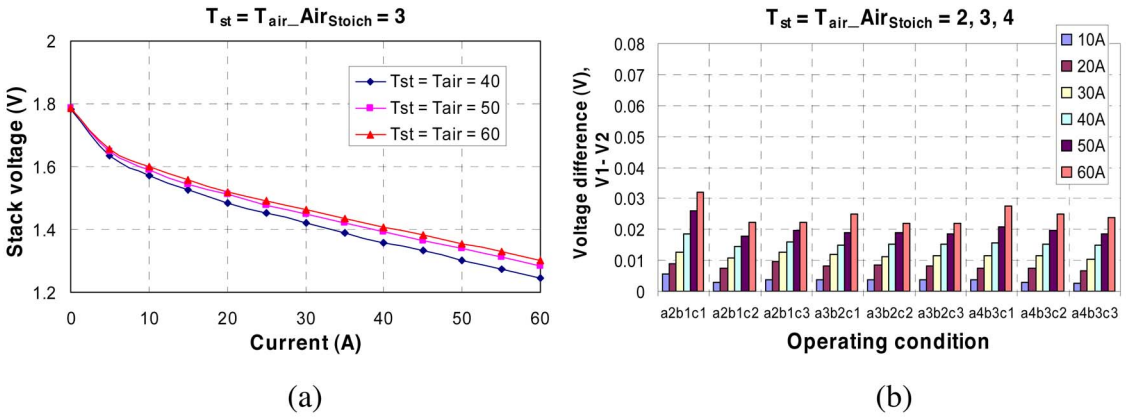

Fig. 5 The stack voltage and the voltage difference under various air stoichiometric ratios at $T_{st} = T_{air}$.

3.1.5 Thermal Circuits. A thermal circuit should be designed to reject excessive heat produced by the stack. Main components of the circuit are a radiator to exchange heat with the ambient, a fan to increase effectiveness of the heat convection, and a reservoir to store and thermally to insulate the coolants. Hence, a coolant pump serves as supplying the coolant to the heat source.

The heat transfer behavior of these components is described by the principle of the thermodynamics. Kroger [25] proposed an empirical equation for a heat transfer coefficient of the radiator h_{rad} (kW/m^2 °C) and pressure drop p_r (kPa) of the radiator as a function of the air flow rate, W_{air} (kg/s):

$$h_{rad} = -1.4495 \cdot W_{air}^2 + 5.9045 \cdot W_{air} - 0.1157$$

$$p_r = (326.12 \cdot W_{air} - 75.396) + 101.325 \quad (10)$$

If the heat of the coolant is fully transferred to the radiator without any losses, the heat capacity of the coolant is identical to the one of the radiator. Thus, the radiator outlet coolant temperature can be expressed as a function of the radiator geometry and the heat convection caused by the temperature difference between the ambient and the radiator outgoing air temperature [26].

$$T_{rad,c,out} = T_{rad,c,in} - 0.5 \cdot \left(\frac{Fr_{area} \cdot (T_{rad,c,in} - T_{amb}) \cdot h_{rad}}{W_c Cp_c} \right) \quad (11)$$

where Fr_{area} is the frontal area (m^2) of the radiator and $T_{rad,c,in}$ is the radiator inlet coolant temperature.

The reservoir should be insulated thermally after a heat exchange at the radiator by the convection. The variation of the heat in the reservoir is the sum of the heat that the coolant carries and the heat being exchanged with the ambient. Accordingly, the reservoir outlet coolant temperature at the end of the given time interval, $T_{res,c,out}$ (K) can be expressed by the following equation [26]:

$$T_{res,c,out} = T_{res,p} - \frac{\Delta t}{M_{res} Cp_{res}} (W_c Cp_c \cdot (T_{res,p} - T_{res,c,in}) + h_{res} A \cdot (T_{res,c,in} - T_{amb})) \quad (12)$$

where $T_{res,p}$ is the temperature of the reservoir at the previous of time step (K), Δt is the time interval (s), M_{res} is an equivalent mass of the coolant in the reservoir (kg), and $T_{res,c,in}$ is the reservoir inlet coolant temperature (K), respectively.

4 Experimental Results and Analyses

4.1 Effects of the Working Temperature of the Stack and the Supplying Air. For the effects of temperature of the stack and the air, two cases have been studied. First, the temperature of the air supplied is set to be equal to the working temperature of the stack. Figure 5(*a*) shows the *I-V* curve dependent on the changes of the temperature at air_{stoich}=3. The *I-V* curves show that the cell voltages increase when the temperature is elevated from 40°C to 60°C. In fact, the elevated working temperature of the stack increases the gas diffusivity and the ionic conductivity in the membrane as long as the hydration of the membrane is kept constant. On the other hand, the water content in the membrane is influenced by the temperature of the air supplied. At an increased water concentration in the cathode gas channel by a higher saturation temperature of the supply air, the water content in the membrane tends to increase. As a result, the ionic conductivity in the membrane gets increased and the associated Ohmic overpotential drops less.

Figure 5(*b*) shows the voltage differences of the two cells at different air_{stoich}. The voltage difference between the two cells tends to increase regardless of the air_{stoich} at a constant working temperature as the load current increases. It turns out that the voltage drop at Cell 2 is larger than the one at Cell 1, even though both cells constructed are apparently supposed to have the same characteristic with the same dimensions and material properties. The difference of the cells voltages between the two cells amounts to 0.01 V at a load current 60 A and air_{stoich}=2 when the temperature of the stack and air is elevated from 40°C to 60°C. In addition, the mean value of the voltage difference has not changed at the same load current, even though the air_{stoich} has been varied, which indicates that the voltage drop in Cell 2 is not affected by the temperature variation. Moreover, the variation of the cell voltages by different air_{stoich} remains identical at different working temperatures of the stack.

When the temperature of the air supplied is equal to the one of the stack, it can be presumed that membranes in both cells are fully humidified, which implies no direct influence of the air flow rate on the voltage drop of Cell 2. Therefore, the difference of the Ohmic overpotentials in Cell 2 can be hypothesized as an inherent characteristic that is possibly given by changes and tolerances made at fabrication of the stack, even though the two cells used the same membrane. Once a stack is designed, it is desirable to derive optimal operating conditions based on this characteristic. The maximum deviation between the two-cell voltages has reached 0.032 V at 60 A.

Second, experiments are conveyed for a case that the temperature of the air stream is different from the one of the stack. Figure 6 shows the experimental results of the *I-V* curve of the stack that indicates no remarkable difference in the stack voltages at a variation of the air temperature (T_{air}=30°C and 40°C) at a constant stack temperature (T_{st}=40°C and 50°C). As matter of fact, the relative humidity at the outlet can be maintained at higher than 80% because of the water produced on the cathode side, when the working temperature of the stack is below 50°C and the pressure

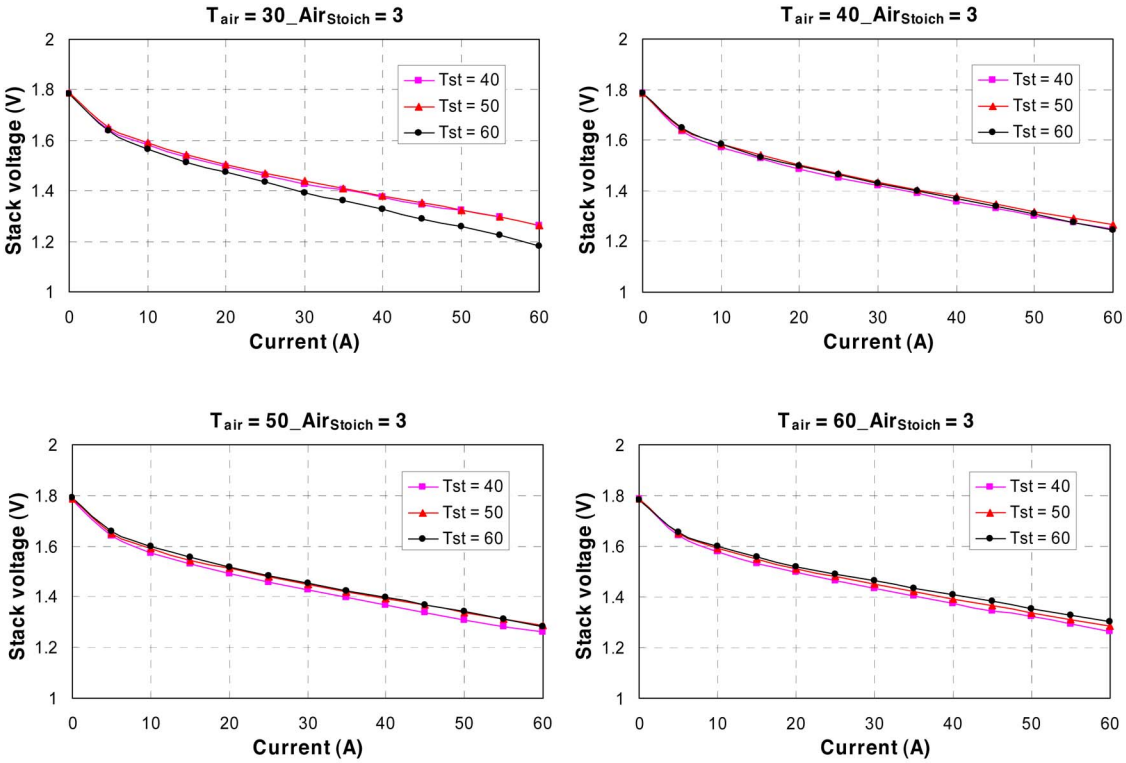

Fig. 6 ***I-V*** **characteristics of the cells and the voltage difference at various T_{air} and T_{st}**

for the cells is operated with 1 atm [27,28]. Thus, the water content in the membrane is not directly affected by the air temperature, even though the air supplied is humidified at a lower temperature than the one of the stack. Under these operating conditions, the humidity on the cathode side is sufficient to maintain the water content in the membrane.

In general, it is anticipated that the voltages of the cells get higher at an elevated temperature. However, the result shows a reversed phenomenon in the voltage at T_{air}=30°C and 40°C. Specifically, the voltage at T_{air}=30°C and T_{st}=60°C shows the lowest amplitude. It indicates that the humidity in the channel cannot be maintained as before when the working stack temperature is higher than 60°C and requires an additional humidification. In addition, when the air with a low vapor pressure is supplied to a stack, the temperature of which is higher than the one of the air, the amount of the water vapor becomes much less than before and the exiting air takes up more water vapor. Subsequently, the membrane might be dehydrated and the Ohmic overpotential gets increased.

Figure 7 shows the experimental results of the stack on the different air_{stoich}. Generally, air_{stoich} influences the partial pressure of the oxygen in the cathode gas channel, water balance in the membrane, and water flooding. When the air_{stoich}=4 is reduced to air_{stoich}=2, the voltage of the stack gets low, which implies that the low air_{stoich} slows down the removal rate of water and raises the level of the water content in the membrane. However, the cell performance at the air_{stoich}=2 is mainly affected by the partial pressure of the oxygen rather than the water content in the membrane. As a result, the cell voltages drop. However, it is to recognize that the voltage becomes lower at T_{st}=60°C, T_{air}=30°C, and air_{stoich}=4, which indicates that the increased flow rate of the air with a low saturation pressure raises the removal rate of water vapor that dehydrates the membrane, even though the partial pressure of the oxygen in cathode gas channel is sufficiently high.

Figure 8 shows the voltage differences between the two cells at different air stoichiometric ratios. At a constant T_{air}, the difference increases as the stack temperature gets higher, while decreasing at a constant T_{st} as the air temperature gets higher. In fact, the elevated temperature of the air results in a higher saturation vapor pressure of the air than the one of the stack channel and subsequently increases the water content in the membrane. Particularly, the voltage drop of Cell 2 is strongly influenced by the amount of the vapor in the air supplied. At T_{st}=60°C and T_{air}=30°C, the voltage drop has reached 0.07 V regardless of the air_{stoich} at a load current of 60 A. In addition, the maximum voltage difference reaches 0.01 V at a variation of air_{stoich} at 60 A. The influence of the air_{stoich} on the voltage difference is comparably small.

5 Comparison Between Simulations and Experiments

5.1 Comparison. Simulations are carried out for a two-cell stack with the model developed. Calculated *I-V* characteristics of the stack as well as the individual cell are compared with the experimental data corrected at a test station installed at the Auburn University. The operating conditions set for the comparison are the same as those in Sec. 2.2.

Figure 9(*d*) shows the simulated and experimented results of the voltage across the stack and Figs. 9(*b*) and 9(*c*) show the cells at two different air temperatures, 30°C and 60°C. The voltages at 60°C show a fair match but a quite difference at the 30°C. The simulation shows that the deviation of the two-cell voltages is not as large as the one measured by the experiment.

Differences in the two cells could be caused by nonuniform characteristics of the individual cells such as reactant distribution and properties of the GDL and the membrane. Effects of the six factors have been taken to investigate in the following sections.

5.2 Sensitivity Analysis for Individual Cell Voltage. The performance of a cell depends on variety of factors that include design parameters and an operating condition. The major design parameters, which possibly changed during fabrication of a stack, are thickness and porosity of the GDL, and thickness of the membrane as well as others that affect the activation overpotentials. In addition, the air distribution is included, which significantly influ-

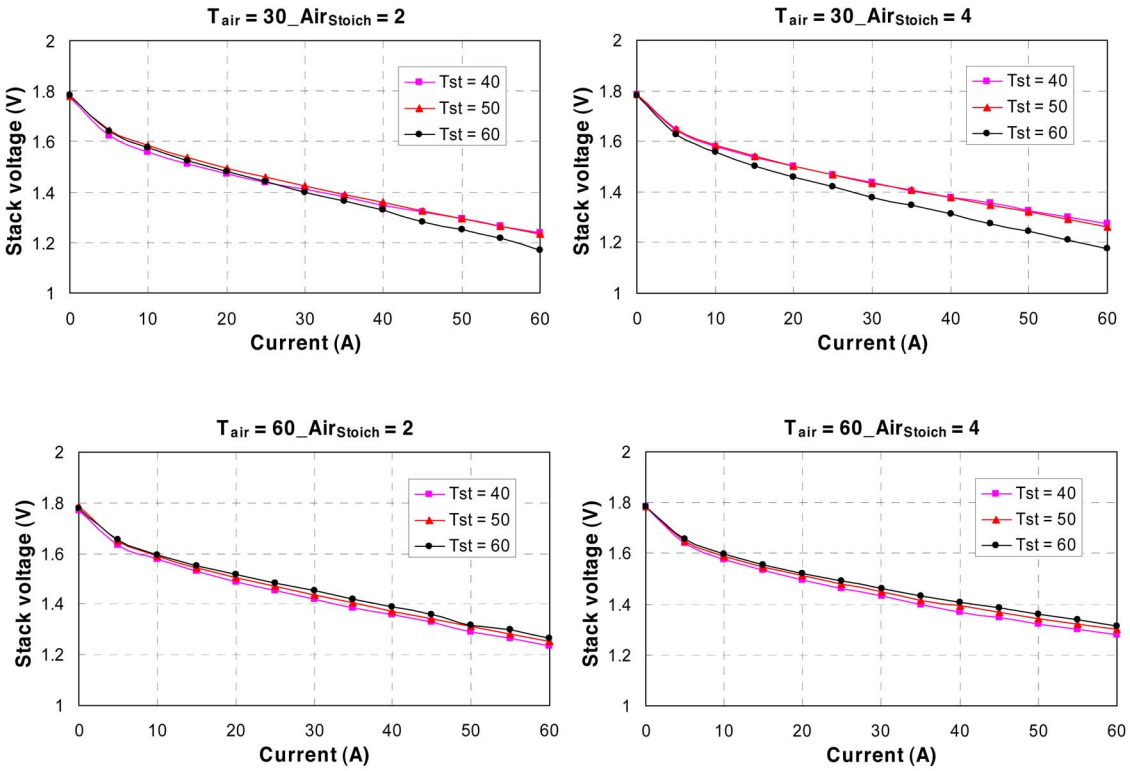

Fig. 7 *I-V* characteristics of the cells and the voltage difference at various T_{air}, T_{st}, and air_{stoich}

ences the performance. According to the results shown above, the voltage in Cell 2 reveals a large discrepancy by comparison. Thus, only the effects of those parameters on the voltage of Cell 2 are compared in detail between the simulated and the experimented results.

5.2.1 Effects of Cathode GDL Thickness and Porosity, Membrane Thickness and Conductivity, and Activation Overpotential. In order to study the sensitivity of design parameters on the performance of Cell 2, thickness of the GDL is changed with a con-

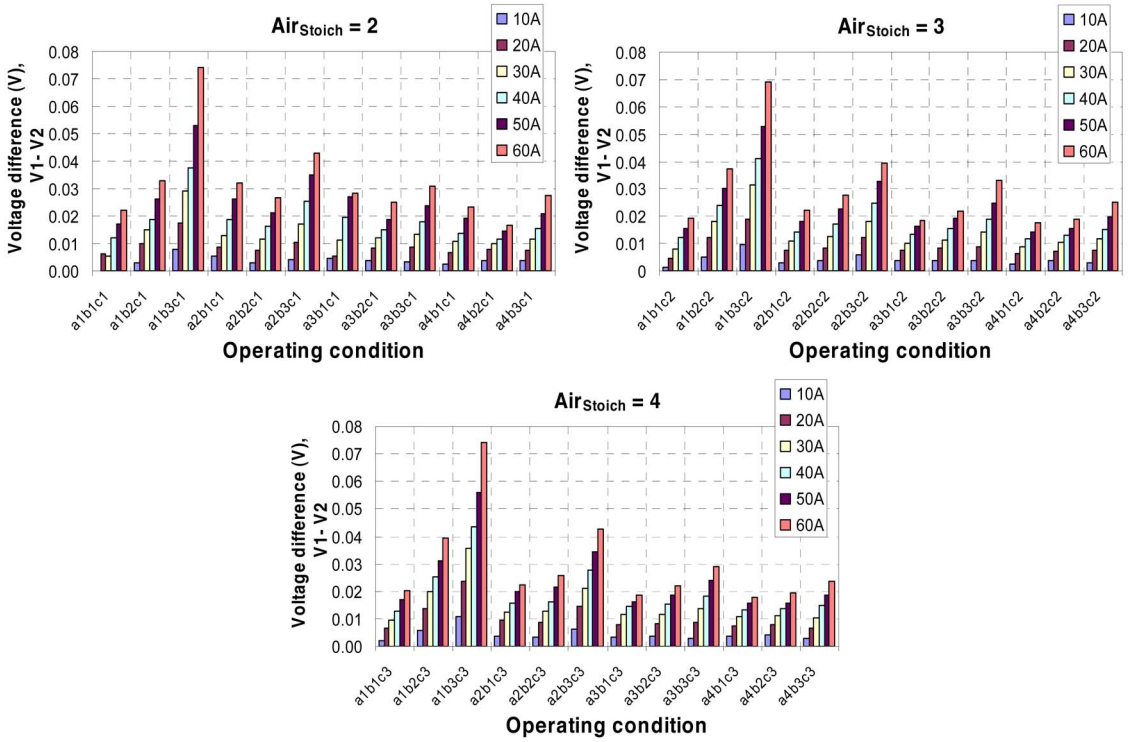

Fig. 8 The voltage difference at various T_{air}, T_{st}, and air_{stoich}

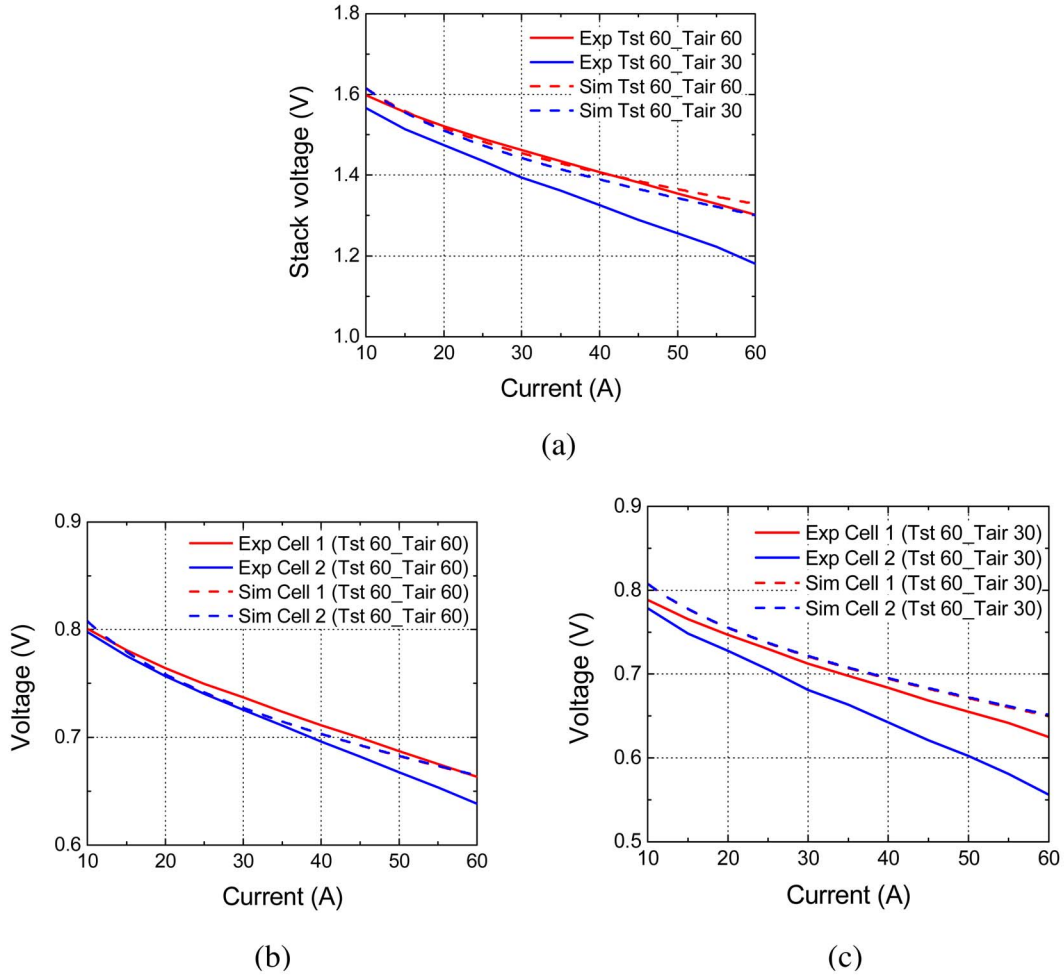

Fig. 9 Comparison of the stack and cell voltages between the experiments and the simulation

stant factor *A* in relation to the one of Cell 1. Then, the performance of the cells is calculated with the model described above. The multiplication factors for Cell 2 are 1.1 and 1.7, respectively, while the thickness for Cell 1 remains the same as before. The performance shown in the Fig. 10 illustrates that no remarkable voltage differences between 1.1 and 1.7 exist under a following operating condition: the stoichiometric ratio=3 and the load current 60 A (0.43 A/cm^2). Presumably, the air will be sufficiently supplied for the low current density.

When the porosity of the GDL is changed, the voltage in the cell is shown in Fig. 11. Factors multiplied for the porosity in Cell 2 are 0.3 and 0.4, while the porosity of Cell 1 is held at 0.5. If the

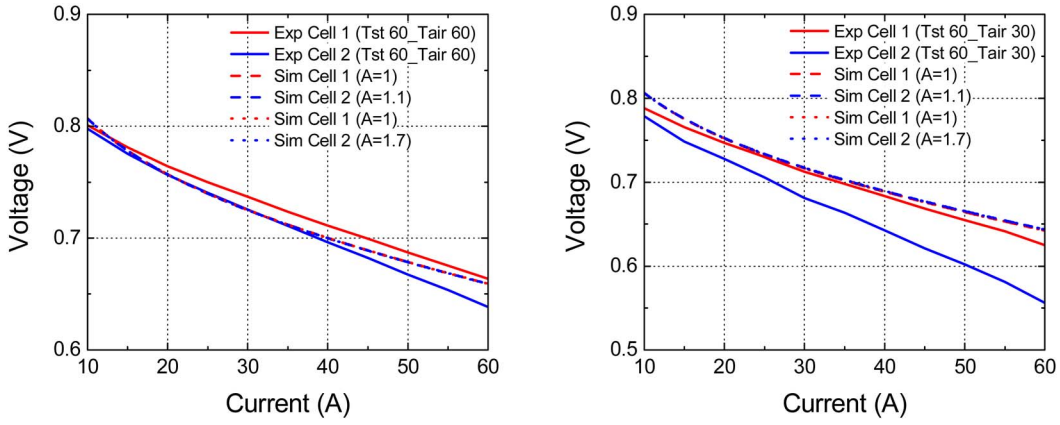

Fig. 10 Sensitivity analyses of the cathode GDL thickness on the cell voltages at different air temperatures

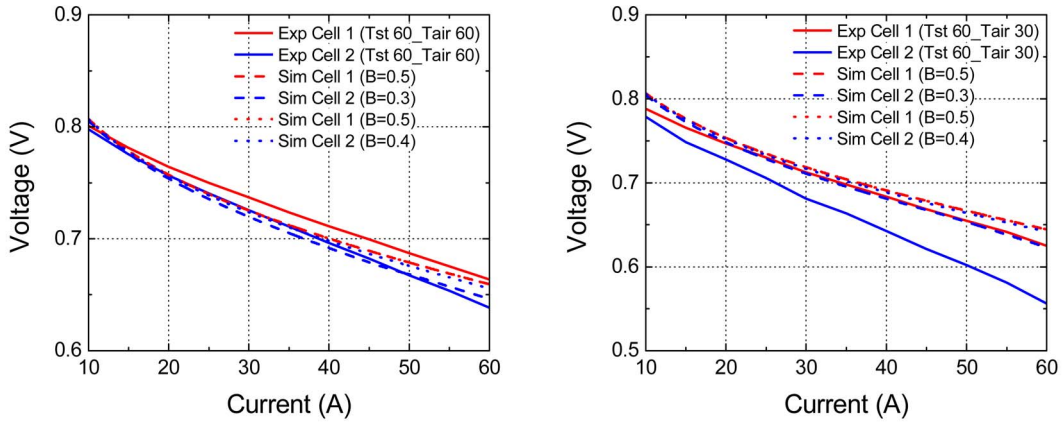

Fig. 11 Sensitivity analyses of the cathode GDL porosity on the cell voltages at different air temperatures

factor for the porosity is smaller than the one of Cell 1, the pressure drop in the layer gets increased and the oxygen concentration in the catalyst gets lower. Thus, the stack voltage is decreased. However, the porosity does not affect the change of the voltage as significantly as the one in the experiment.

In general, membranes are a part of the MEA. Thus, the thickness of the membrane cannot be measured precisely in an assembled stack. In this study, it is assumed that the MEA is constructed with two separable layers of a catalyst and a membrane, the thickness of which can be varied with a factor, C. The factors considered are 1.1 and 1.5, respectively. The I-V curve of the cell is shown in Fig. 12. As a membrane gets thicker, the Ohmic resistance gets increased and the voltage drop gets increased. However, the thickness does not affect the change of the voltage as significant as the one in the experiment.

The effects of the membrane properties on the performance are very complex. One of the parameters that strongly influence the Ohmic overpotential is the proton conductivity that has been changed with a ratio of D. Figure 13 shows the variation of the cell voltages at two different air temperatures. When D is decreased, the voltage in Cell 2 tends to be lower than the one in Cell 1. As the current density increases, the deviation of the voltages between Cell 1 and 2 gets larger and follows the trend that the experimental data have shown.

Coefficients used for description of the activation overpotential are affected by many design parameters and empirical values [11]. Thus, a factor is multiplied to the overall overpotential in the analysis. Figure 14 shows the voltage of Cell 2, which decreases as E increases. However, the deviation of the voltage is constant regardless of the amplitude of the current density. In addition, it is observed that the deviation width of the voltage drop has not been changed regardless of the T_{air} that is decreased from the 60°C to 30°C.

5.2.2 Effect of Air Distribution. The current model assumed a uniform distribution of the air in the gas flow channel for both cells. The uniformity of the air flow in both cells is hardly to measure in a real system. In order to study the sensitivity of the nonuniform air distribution on the I-V curve of the stack, the air flow rate supplied to the cells has been changed with a ratio, F.

Figure 15 shows the cell voltages at the different ratios of the air flow rate. At 60°C of the air temperature, the cell voltage with a high air flow rate tends to increase because of the increased partial pressure of the oxygen. In contrast, the cell voltage gets decreased at the 30°C of the air temperature, which indicates that the increased flow rate of the air at a low saturation pressure raises the removal rate of water vapor that dehydrates the membrane, even though the partial pressure of the oxygen in the cathode gas channel is sufficiently high. It can be concluded that the air flow rate does not significantly affect the variation of the voltage of Cell 2. The voltage difference in the simulation is comparably small in comparison to the experiment.

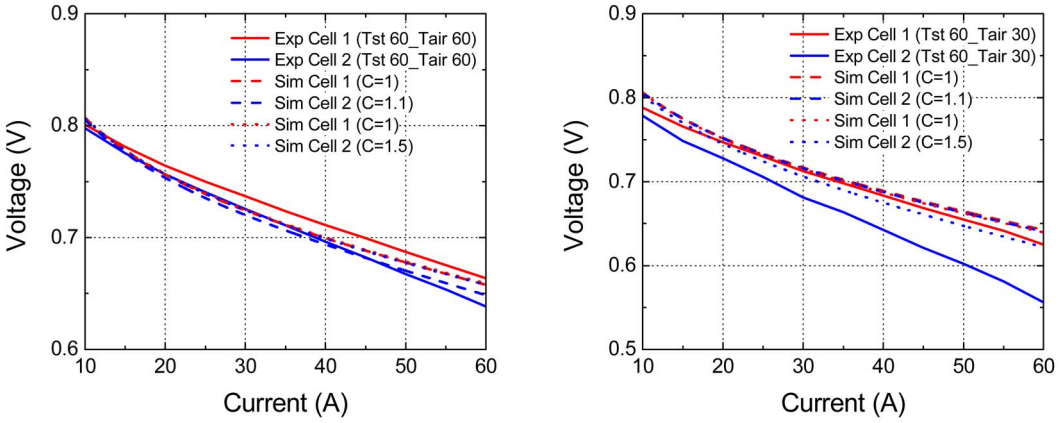

Fig. 12 Sensitivity analyses of the membrane thickness on the cell voltages at different air temperatures

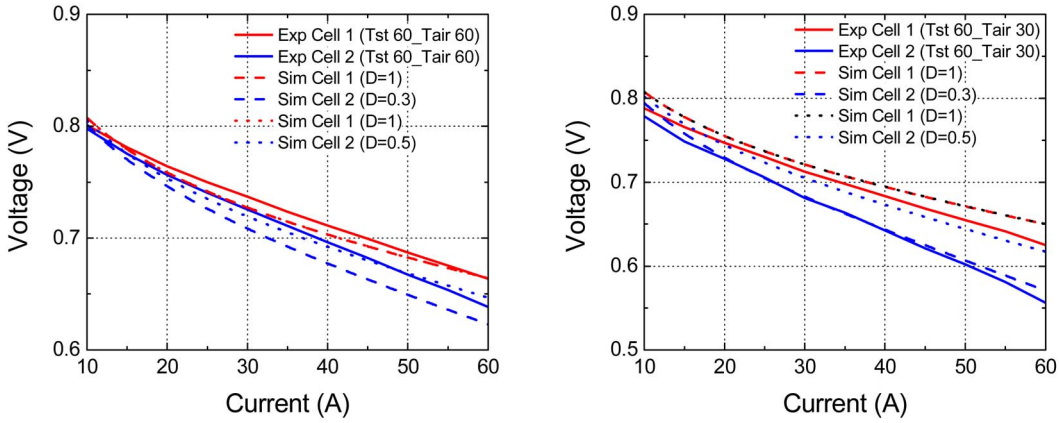

Fig. 13 Sensitivity analyses of the proton conductivity on the cell voltages at different air temperatures

6 Conclusions

The paper presented focuses on experimental measurements and analyses of the individual cell voltages of a stack based on a dynamic model developed under different operating conditions. The results are summarized as follows:

- Even at $T_{st}=T_{air}$, there exists a voltage difference between the two cells, which can be regarded as Ohmic overpotential inherently given by different characteristics of the components used and tolerances occurring during fabrication of the stack. The voltage difference at the stack amounts to 0.032 V at a load current of 60 A.
- Due to the relatively low load current density applied to the stack, no water flooding phenomena have been observed in the experiments. The temperature of the air stream among other operating variables showed the most influential factor in manipulating the voltage of the cells. It shows that the difference of the cell voltages gets smaller when the work-

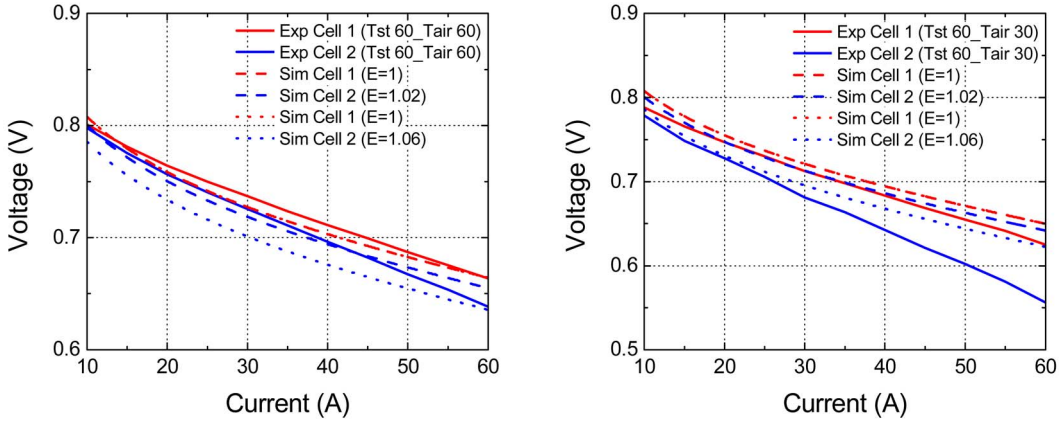

Fig. 14 Sensitivity analyses of the activation over-potential on the cell voltages at different air temperatures

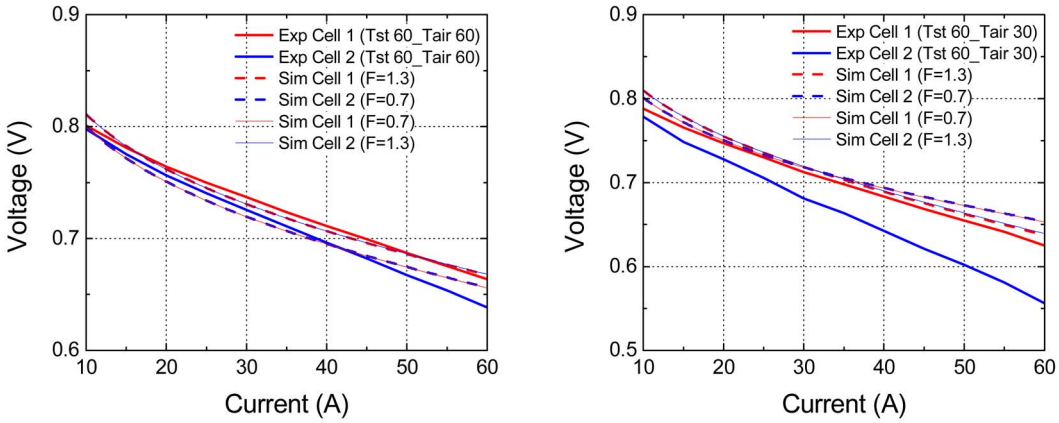

Fig. 15 Sensitivity analyses of the air flow rate on the cell voltages at different air temperatures

ing temperature of the stack is elevated, while the air_{stoich} has the least influence. At $T_{air}=30\,^{\circ}C$ and $T_{st}=60\,^{\circ}C$, the difference of the cell voltages has been increased to 0.074 V at a load current of 60 A.

- The stoichiometric ratio does not significantly influence the overall voltage difference, even though the voltage difference reached 0.01 V at the load current of 60 A.
- Results of simulations do not show a voltage deviation at a variation of the air temperature because the inherent characteristic is not reflected.
- Sensitivity analyses reveal that variation of proton conductivity of the membrane is the most significant parameter that approximates the experimental results of the cell voltage.

References

[1] Wöhr, M., Bolwin, K., Schnurnberger, W., Fischer, M., Neubrand, W., and Eigenberger, G., 1998, "Dynamic Modeling and Simulation of a Polymer Membrane Fuel Cell Including Mass Transport Limitation," Int. J. Hydrogen Energy, **23**, pp. 213–218.

[2] Yan, Q., Toghiani, H., and Causey, H., 2006, "Steady State and Dynamic Performance of Proton Exchange Membrane Fuel Cells (PEMFCs) Under Various Operating Conditions and Load Changes," J. Power Sources, **161**, pp. 492–502.

[3] Santarelli, M. G., and Torchio, M. F., 2007, "Experimental Analysis of the Effects of the Operating Variables on the Performance of a Single PEMFC," Energy Convers. Manage., **48**, pp. 40–51.

[4] Wang, L., and Liu, H., 2004, "Performance Studies of PEM Fuel Cells With Interdigitated Flow Fields," J. Power Sources, **134**, pp. 185–196.

[5] Wang, L., Husar, A., Zhou, T., and Liu, H., 2003, "A parametric Study of PEM Fuel Cell Performances," Int. J. Hydrogen Energy, **28**, pp. 1263–1272.

[6] Hwang, J. J., and Hwang, H. S., 2002, "Parametric Studies of a Double-Cell Stack of PEMFC Using Grafoil™ Flow-Field Plates," J. Power Sources, **104**, pp. 24–32.

[7] Wahdame, B., Candusso, D., and Kauffmann, J. M., 2006, "Study of Gas Pressure and Flow Rate Influences on a 500 W PEM Fuel Cell, Thanks to the Experimental Design Methodology," J. Power Sources, **156**, pp. 92–99.

[8] Yan, W. M., Mei, S. C., Soong, C. Y., Liu, Z. S., and Song, D., 2006, "Experimental Study on the Performance of PEM Fuel Cells With Interdigitated Flow Channels," J. Power Sources, **160**, pp. 116–122.

[9] Buchi, F. N., and Scherer, G. G., 1996, "In Situ Resistance Measurements of Nafion® 117 Membranes in Polymer Electrolyte Fuel Cells," J. Electroanal. Chem., **404**, pp. 37–43.

[10] Anantaraman, A. V., and Gardner, C. L., 1996, "Study on Ion-Exchange Membranes. Part 1. Effect of Humidity on Conductivity of Nafion®," J. Electroanal. Chem., **414**, pp. 155–120.

[11] Amphlett, J. C., Baumert, R. M., Mann, R. F., Peppley, B. A., and Roberge, P. R., 1995, "Performance Modeling of the Ballard Mark IV Solid Polymer Electrolyte Fuel Cell. I. Mechanistic Model Development," J. Electrochem. Soc., **142**, pp. 1–8.

[12] Williams, M. V., Kunz, H. R., and Fenton, J. M., 2004, "Operation of Nafion®-Based PEM Fuel Cells With No External Humidification: Influence of Operating Conditions and Gas Diffusion Layers," J. Power Sources, **135**, pp. 122–134.

[13] Amphlett, J. C., Baumert, R. M., Mann, R. F., Peppley, B. A., and Roberge, P. R., 1995, "Performance Modeling of the Ballard Mark IV Solid Polymer Electrolyte Fuel Cell. II. Empirical model Development," J. Electrochem. Soc., **142**, pp. 9–15.

[14] Springer, T. E., Zawodzinski, T. A., and Gottesfeld, S., 1991, "Polymer Electrolyte Fuel Cell Model," J. Electrochem. Soc., **138**, pp. 2334–2341.

[15] Torchio, M. F., and Santarelli, M. G., 2005, "Experimental Analysis of the CHP Performance of a PEMFC Stack by a 2^4 Factorial Design," J. Power Sources, **149**, pp. 33–43.

[16] Ferng, Y. M., Tzang, Y. C., Pei, B. S., Sun, C. C., and Su, A., 2004, "Analytical and Experimental Investigations of Proton Exchange Membrane Fuel Cell," Int. J. Hydrogen Energy, **29**, pp. 381–391.

[17] Mennola, T., Mikkola, M., Noponen, M., Hottinen, T., and Lund, P., 2002, "Measurement of Ohmic Voltage Losses in Individual Cells of a PEMFC Stack," J. Power Sources, **112**, pp. 261–272.

[18] Yuan, X., Sun, J. C., Wang, H., and Zhang, J., 2006, "AC Impedance Diagnosis of a 500 W PEM Fuel Cell Stack Part II: Individual Cell Impedance," J. Power Sources, **161**, pp. 929–937.

[19] Rodatz, P., Buchi, F., Onder, C., and Guzzella, L., 2004, "Operational Aspects of a Large PEFC Stack Under Practical Conditions," J. Power Sources, **128**, pp. 208–217.

[20] Nguyen, T. V., and White, R. E., 1993, "A Water and Heat Management Model for Proton-Exchange-membrane Fuel Cells," J. Electrochem. Soc., **140**, pp. 2178–2186.

[21] Mo, Z. J., Zhn, X. J., Wei, L. Y., and Cao, G. Y., 2006, "Parameter Optimization for a PEMFC Model With a Hybrid Genetic Algorithm," Int. J. Energy Res., **30**, pp. 585–597.

[22] Nam, J. H., and Kaviany, M., 2003, "Effective Diffusivity and Water-Saturation Distribution in Single and Two-Layer PEMFC Diffusion Medium," Int. J. Heat Mass Transfer, **46**, pp. 4595–4611.

[23] McKay, D. A., Ott, W. T., and Stefanopoulou, A. G., 2005, "Modeling, Parameter Identification, and Validation of Reactant and Water Dynamics for a Fuel Cell Stack," ASME Paper No. IMECE2005-81484.

[24] Shan, Y., and Choe, S. Y., 2005, "A High Dynamic PEM Fuel Cell Model With Temperature Effects," J. Power Sources, **145**, pp. 30–39.

[25] Kroger, D. G., 1984, "Radiator Characterization and Optimization," SAE Paper No. 840380.

[26] Gurski, S., 2002, "Cold Start Effects on Performance and Efficiency for Vehicle Fuel Cell System," Master thesis, Virginia Polytechnic Institute and State University, Blacksburg.

[27] Williams, M. V., Kunz, H. R., and Fenton, J. M., 2004, "Operation of Nafion®-Based PEM Fuel Cells With No External Humidification: Influence of Operating Conditions and Gas Diffusion Layers," J. Power Sources, **135**, pp. 122–134.

[28] Larminie, J., and Dicks, A., 2003, *Fuel Cell Systems Explained*, 2nd ed., Wiley, New York.